



Numerical investigation of the effect of ocean depth variations on the dynamics of a ship mounted two-DoF manipulator system

Mohamad Luthfi Ramadiansyah^{a, *}, Edwar Yazid^a, Cheng Yee Ng^b

^a Research Center for Smart Mechatronics, National Research and Innovation Agency (BRIN)
Kawasan Bandung Cisit, Jl. Sangkuriang, Dago, Coblong, Bandung, 40135, Indonesia

^b Department of Civil and Environmental Engineering, Universiti Teknologi PETRONAS
32610 Seri Iskandar, Perak, Malaysia

Received 17 October 2022; Revised 16 November 2022; Accepted 17 November 2022; Published online 29 December 2022

Abstract

The dynamics of a ship need to be considered in the development of a manipulator system that will be applied to the ocean-based operation. This paper aims to investigate the effect of ocean depth variations on the ship motion as disturbances to a ship-mounted two-DoF (Degrees of Freedom) manipulator joint torque using an inverse dynamics model. Realization is conducted by deriving the mathematical model of a two-DoF manipulator system subject to six-DoF ship motion, which is derived by using Lagrange-Euler method. It is then combined with numerical hydrodynamic simulation to obtain the ship motions under ocean depth variations, such as shallow (50 m), intermediate (750 m), and deep (3,000 m) waters. Finding results show that randomness of the ship motions appears on the manipulator joint torque. In the azimuth link, maximum joint torque is found in shallow water depth with an increment of 8.271 N.m (285.69 %) from the undisturbed manipulator. Meanwhile, the maximum joint torque of the elevation link is found in intermediate water depth with an increment of 53.321 N.m (6.63 %). However, the difference between depth variations is relatively small. This result can be used as a baseline for sizing the electrical motor and developing the robust control system for the manipulator that is mounted on the ship by considering all ocean depth conditions.

©2022 National Research and Innovation Agency. This is an open access article under the CC BY-NC-SA license (<https://creativecommons.org/licenses/by-nc-sa/4.0/>).

Keywords: two-DoF manipulator; inverse dynamics; ship motion; ocean depth; hydrodynamic response.

I. Introduction

It is widely known that robotic systems may be easily found in many engineering applications. Design and analysis of such a system has been carried out in some areas, such as industrial application [1][2], underwater [3], vehicle [4], satellite antenna [5], and humanoid robot [6][7] with their specified objectives. The essential task in developing a robotic system is kinematics and dynamics modeling. Kinematics modeling is commonly carried out to determine the position and orientation of manipulator links. Tavassolian *et al.* [8] had employed the forward kinematics model of a parallel robot using a combined method based on the neural network. Dewandhana *et al.* [9] had

similar work but with a different application, i.e., a full-arm robot. Inverse kinematics had been performed by Kusmenko and Schmidt [10] for developing a 5-DoF (Degrees of Freedom) robot arm and by Chen *et al.* [11] for an underwater propeller cleaning application. Amundsen *et al.* [12] had performed inverse kinematics for manipulator control that was implemented on a non-fixed based.

Inverse dynamics model is commonly used to obtain the dynamic characteristics of a manipulator system. It was implemented by Polydoros *et al.* [13] for torque control manipulator, Awatef and Mouna [14] for motion control of the unicycle mobile robot, and Crenna and Rossi [15] for measurement of internal torques in the articulations of the human body during a gesture. The calculation of inverse dynamics using computational methods is currently well-known for its efficient purpose. Farah and Shaogang [16] had introduced an efficient approach

* Corresponding Author. Tel: +62-878-2460-7227
E-mail address: moha057@brin.go.id

for modeling robot dynamics. They used Matlab and SimMechanics instead of an analytical approach, but the study was limited to ground-based applications. Meanwhile, Müller [17] had compared classical and computational methods.

Besides to fulfill its function, the development of a robotic system must consider the behavior of its base, in which the system will be operated. Dynamics of the non-inertial base certainly affect the positioning of manipulator arms which is the main task of a robotic system. Wei *et al.* [18] had performed a dynamic analysis of a mobile manipulator that operated on the 3-DoF floating base. Similar work of non-inertial base manipulator had been done by [19], which introduced the modeling and control of a soft robotic arm on the aerial vehicle.

To the best of the author's knowledge, dynamic analysis of a manipulator excited by ship motions is relatively rare. Some literature that relates to this topic may be found in [20][21][22], although they mainly focused on the control system development. Research by Qian and Fang in [23] is regarded as the closest work where they had analyzed the regular ocean waves effect to the dynamic analysis of a ship-mounted crane system. Further, dynamics of manipulator systems subject to irregular ocean waves induced ship motions had been performed by [24] under variations of sea states. Important finding results show that the maximum joint torque of a manipulator is proportional to the increment of significant wave height and greatly affected by the direction of ocean wave propagation. To date, there has not yet been research working on the effect of ocean depths on manipulator dynamics. Ahmed *et al.* [25] presented that the water particle force on the oceanic structure depends on the ocean depth. Hence, this paper investigates the effect of ocean depth variations on the manipulator joint torque with contributions as follows:

- To develop a mathematical model of a ship-mounted two-DoF manipulator considering the ship dynamics.
- To characterize the ship motions as excitations

to the base of a manipulator system subject to random ocean waves under variations of ocean depth using numerical hydrodynamic simulation and propose its methodology.

- To perform a parametric study in terms of variations of ocean depth to the manipulator dynamics.

This paper is organized as follows: system description and the underlying method, as well as the governing equations, are described in Section II. Results and discussions of derived governing equations, numerical simulations, and manipulator dynamic characteristics are presented in Section III. Conclusion and recommendations are put in Section IV.

II. Materials and Methods

The underlying manipulator construction is illustrated in Figure 1, where it has two degrees of freedom, namely azimuth and elevation links. The former is designed to be able to fully rotate in the horizontal plane with a maximum angle of 360° C(C)W, while the elevation angle can rotate in the vertical plane with a range angle at -20° ~ 60° C(C)W. The end-effector is designed to aim and lock on the target on the ocean water surface. A control system must be applied to move the arms at certain angles precisely when the base of the manipulator is excited by random ocean waves induced ship motions. This is in order to enable the end-effector to stick to the target. Moreover, ship motions are treated as a six-DoF rigid body, as visualized in Figure 2 under non-propelled conditions. Respectively in the X, Y, and Z axis, translational motions are called Surge, Sway, and Heave, and rotational motions are Roll, Pitch, and Yaw. To calculate manipulator joint torque, the inverse dynamics model is applied, and the process flow is shown in Figure 3. The ship motions can be measured with a motion sensor unit, which has three accelerometers for detecting surge, sway, and heave and three rotation rate sensors for measuring roll, pitch, and yaw [26]. In this paper, a combination

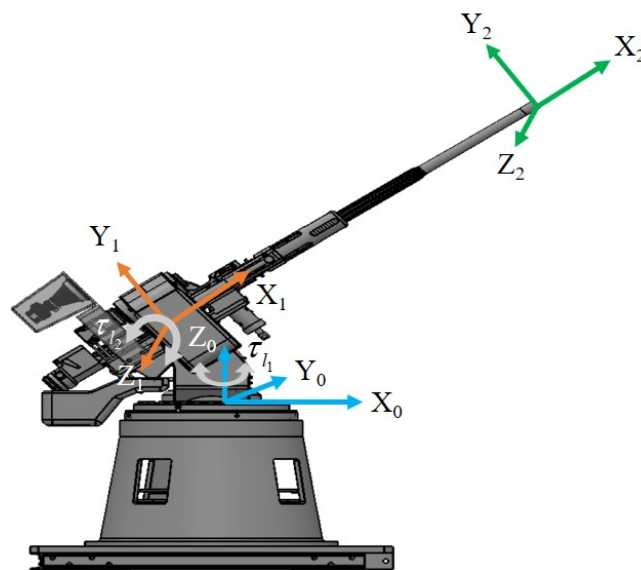


Figure 1. Schematic of a manipulator system

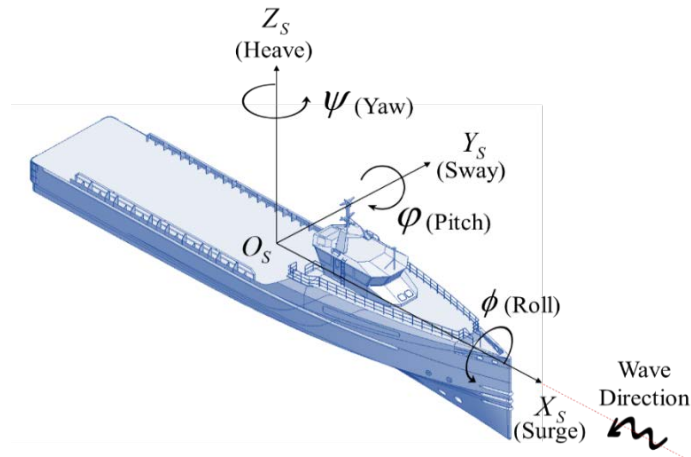


Figure 2. Visualization of ship motions

of analytical and numerical methods is proposed to simulate ship motions and manipulator joint trajectory from the sensor system. The former is analytical simulations of joint trajectory and manipulator dynamics, and the latter is a numerical simulation of the ship motions using ANSYS Aqwa in the variations of ocean depth. Here, equations of motion of a ship-mounted manipulator system are derived by using Lagrange-Euler method. Thus, discussion with regard to control system design and analysis, including sensor system, is out of this paper's range. To begin with, the main parameters of the manipulator system and ship geometry are given with certain conditions applied.

A. Forward kinematics

Kinematics of a ship-mounted manipulator system as an early step in the dynamic analysis is realized in the form of forward and inverse kinematics. The former is defined from the base to the end-effector using manipulator joint parameters and coordinates, as noted in Figure 1. A homogeneous transformation matrix of the system is then built based on the widely adopted Denavit-Hartenberg (DH) method [27] by multiplying each homogeneous transformation matrix of the joint from the base into the end-effector. Homogeneous

transformation matrix (T) consists of a rotational matrix (R) and position matrix (P), which is defined as equation (1),

$$T = \begin{bmatrix} R_{n,s,a} & P_{X,Y,Z} \\ 0 & 1 \end{bmatrix} = \begin{bmatrix} n_x & s_x & a_x & P_x \\ n_y & s_y & a_y & P_y \\ n_z & s_z & a_z & P_z \\ 0 & 0 & 0 & 1 \end{bmatrix} \quad (1)$$

The terms, s and a denote normal, shear, and approach vectors in the XYZ-axes. Using manipulator frame coordinates in Figure 1, the total homogeneous transformation matrix can be written as equation (2),

$$H = T_s \cdot T_M \quad (2)$$

The term H is the total, T_s is the ship, and T_M is the manipulator homogeneous transformation matrices, respectively. The homogeneous transformation matrix of a ship can be expressed as equation (3),

$$T_s = \begin{bmatrix} c\psi c\phi & c\psi s\phi s\phi - s\psi c\phi & c\psi c\phi s\phi + s\psi s\phi & X_s \\ s\psi c\phi & s\phi s\phi s\psi + c\psi c\phi & s\phi s\psi c\phi - c\psi s\phi & Y_s \\ -s\phi & c\phi s\phi & c\phi c\phi & Z_s \\ 0 & 0 & 0 & 1 \end{bmatrix} \quad (3)$$

The term c and s represent \cos and \sin ; X_s , Y_s , and Z_s are the translational ship motions, such as surge,

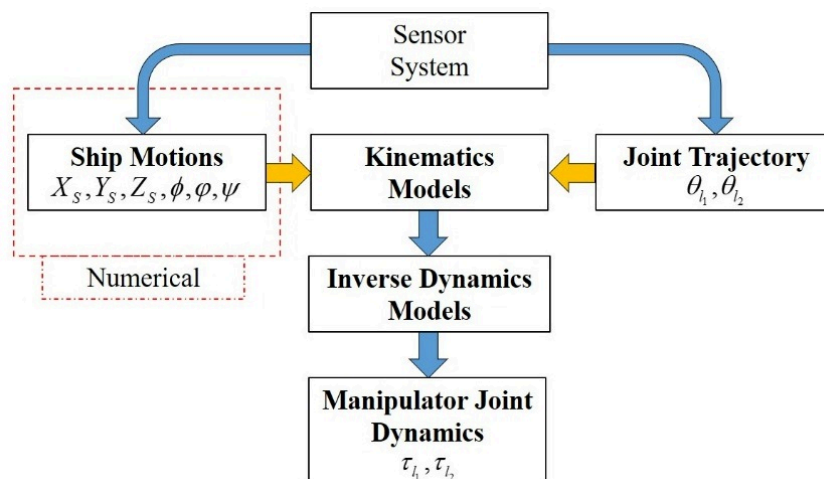


Figure 3. Steps for simulating the inverse dynamics of a manipulator system

sway, and heave, respectively; and ϕ , φ , and ψ are the rotational ship motions, namely roll, pitch, and yaw, respectively. The homogeneous transformation matrix of manipulator system can be written as equation (4) and equation (5),

$${}^0_2T_M = {}^0_1T_M \cdot {}^1_2T_M \quad (4)$$

$${}^{i-1}_i T_M = \begin{bmatrix} c\theta_{l_i} & -s\theta_{l_i} & 0 & a_{i-1} \\ c\alpha_{i-1}s\theta_{l_i} & c\alpha_{i-1}c\theta_{l_i} & -s\alpha_{i-1} & -s\alpha_{i-1}d_i \\ s\alpha_{i-1}s\theta_{l_i} & c\theta_{l_i}s\alpha_{i-1} & c\alpha_{i-1} & -c\alpha_{i-1}d_i \\ 0 & 0 & 0 & 1 \end{bmatrix} \quad (5)$$

The term ${}^{i-1}_i T_M$ is the transformation matrix from the $i-1$ frame to i frame, θ_i is joint angle, α_{i-1} is the rotational link angles in X-axis, a and d are respective link distances in the X- and Z-axes. Using manipulator kinematic parameters of the link in Table 1, equation (5) can be rewritten for each joint as equation (6) and equation (7),

$${}^0_1T_M = \begin{bmatrix} c\theta_{l_1} & -s\theta_{l_1} & 0 & 0 \\ s\theta_{l_1} & c\theta_{l_1} & 0 & 0 \\ 0 & 0 & 1 & 0 \\ 0 & 0 & 0 & 1 \end{bmatrix} \quad (6)$$

$${}^1_2T_M = \begin{bmatrix} c\theta_{l_2} & -s\theta_{l_2} & 0 & 0 \\ 0 & 0 & -1 & 0 \\ s\theta_{l_2} & c\theta_{l_2} & 0 & 0 \\ 0 & 0 & 0 & 1 \end{bmatrix} \quad (7)$$

B. Inverse dynamics

An inverse dynamics model is used to define the manipulator joint torque with predefined joint trajectories. The torque can be expressed in several terms, such as inertia, centrifugal, Coriolis, and gravity as equation (8),

$$\tau = M(\theta)\ddot{\theta} + V(\theta, \dot{\theta}) + G(\theta) \quad (8)$$

The term τ is manipulator joint torque, M is the mass matrix that contributes to the torque due to inertia, V is the matrix of centrifugal and Coriolis terms, and G is the matrix of gravity term [28]. Recall the Euler's equation, the torque value is defined as equation (9),

$$\frac{d}{dt} \frac{\partial L}{\partial \dot{\theta}} - \frac{\partial L}{\partial \theta} = \tau \quad (9)$$

$$L(\theta, \dot{\theta}) = K(\theta, \dot{\theta}) - P(\theta) \quad (10)$$

The term L is the Lagrange operator, θ is position, $\dot{\theta}$ is velocity, and $\ddot{\theta}$ is acceleration of the joint. Lagrange formulation is defined as the difference between kinetic energy (K) and potential energy (P) following equation (10). Substituting equation (10) into equation (9), it can be written as equation (11),

$$\tau_i = \frac{d}{dt} \frac{\partial K_i}{\partial \dot{\theta}} - \frac{\partial K_i}{\partial \theta} + \frac{\partial P_i}{\partial \theta} \quad (11)$$

Kinetic energy is obtained from translational and rotational motions, while potential energy is due to gravity effect as equation (12) and equation (13),

$$K_i = \frac{1}{2} m_i v_c^T v_c + \frac{1}{2} {}^i \omega_i^T I_i {}^i \omega_i \quad (12)$$

$$P_i = m_i g^T {}^0 P_c \quad (13)$$

The term m_i is mass, v_c is linear velocity at the centre of gravity, ω is angular velocity, I is the moment of inertia of the link, g is gravity, and P_c is position matrix from the homogeneous transformation matrix. All variables in equations (12)(13) are transformed into matrix form where the mass and moment of inertia of each link follow the manipulator design parameters. Linear and angular velocities can be obtained from velocity propagation as equation (14) and equation (15),

$${}^{i+1} v_{i+1} = {}^{i+1}_i R ({}^i v_i + {}^i \omega_i \times {}^i P_{i+1}) + \dot{d}_{i+1} {}^{i+1} \hat{Z}_{i+1} \quad (14)$$

$${}^{i+1} \omega_{i+1} = {}^{i+1}_i R {}^i \omega_i + \dot{\theta}_{i+1} {}^{i+1} \hat{Z}_{i+1} \quad (15)$$

The term R is rotational matrix from homogeneous transformation matrix, \dot{d} is linear velocity, $\dot{\theta}$ is angular velocity, and \hat{Z} is direction vector of the joint. It should be noted that the manipulator joint motion is predefined using a 5th-order spline function.

C. Ship Motions

Ship motions are carried out by numerical simulation using commercial software. In this paper, ANSYS Aqwa is employed to simplify the process from the ship modelling until the ship motions analysis. This type of software provides a toolset for investigating the effects of environmental loads on floating and fixed offshore as well as marine structures. This software can also be used to analyze the hydrodynamic diffraction and responses of a body subject to ocean waves. Overall, hull modelling, meshing process, and ocean waves generation subject to the ocean depth are evaluated by ANSYS Aqwa.

1) Ship hull modelling

In practice, a ship model can be simplified into a hull model, which can be seen in Figure 4. The hull interacts with ocean waves so that it becomes the main geometry that must be modeled properly. In Aqwa, modelling is based on surface geometry that may be designed from a geometry editor in ANSYS or other modelling softwares in the form of *.stp or *.igs files. In this paper, Solidworks in *.stp format is used and then imported into a geometry editor in Aqwa.

2) Meshing process

The meshing process is performed in Aqwa. Boundary conditions and parameters of the ship are tabulated in Table 2. However, the current meshing process is different from the common CFD mesh, where the working fluid is set as the object. Here, the ship hull is the mesh object, as seen in Figure 5. It shows the surface mesh of the ship hull and the

Table 1.
Manipulator kinematic parameters

i	θ_i	α	a	d
1	θ_{l_1}	0	0	0
2	θ_{l_2}	90°	0	0
3	0	0	0	r

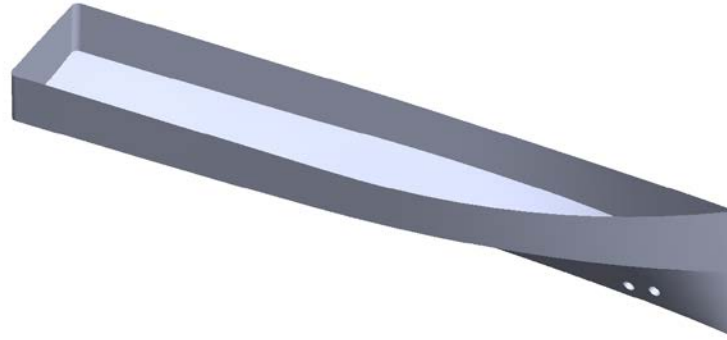


Figure 4. Geometry of ship hull surface

grid independence test result that corresponds to the hydrostatic heave as the parameter for determining the effective total elements. At the 22,210 elements, the hydrostatic value has approached the correct value and it becomes the meshing parameter hereafter. Using the higher elements can result in long-time iteration in the simulation process.

3) Ship and ocean random waves interaction modelling

Random ocean waves are applied rather than regular ocean waves since they represent the actual ocean waves. Adopted from Linear airy wave theory [29], random ocean wave height is a summation of regular waves with different frequencies. JONSWAP type spectrum is used, which is the standard ocean wave model and more versatile than other spectrums. Its spectral ordinate at a frequency (ω) is expressed as equation (16),

$$S(\omega) = \alpha H_s^2 \left(\frac{\omega_p}{\omega}\right)^5 \exp\left(-\frac{5}{4}\left(\frac{\omega_p}{\omega}\right)^4\right) \gamma \exp\left(-\frac{(\omega-\omega_p)^2}{2\sigma^2\omega_p^2}\right) \quad (16)$$

The term α is a Phillip's constant, H_s is significant wave height, ω_p is peak frequency, γ is peakedness parameter, σ is shape parameter [24]. By taking the values of spectral ordinate $S(\omega)$, the amplitude of the

i^{th} ocean wave component can be calculated by using equation (17),

$$a_i = \sqrt{2S(\omega_i)\Delta\omega} \quad (17)$$

From equation (17) and the values of a_i , the time series of wave height can be generated as equation (18),

$$\xi(x, y, t) = \sum_{i=0}^N a_i \sin(\omega_i t + \theta_i - k_i x \cos \chi - k_i y \sin \chi) \quad (18)$$

The term ξ is wave elevation, N is number of wave component, k is wave number, and χ is wave propagating direction. From linear wave theory, wave particle kinematics can be expressed as equations (19)–(23),

$$v_x = \omega \zeta_a \frac{\cosh[k(z+h)]}{\sinh(kh)} \cos(kx - \omega t) \quad (19)$$

$$v_z = \omega \zeta_a \frac{\sinh[k(z+h)]}{\sinh(kh)} \sin(kx - \omega t) \quad (20)$$

$$a_x = \omega^2 \zeta_a \frac{\cosh[k(z+h)]}{\sinh(kh)} \sin(kx - \omega t) \quad (21)$$

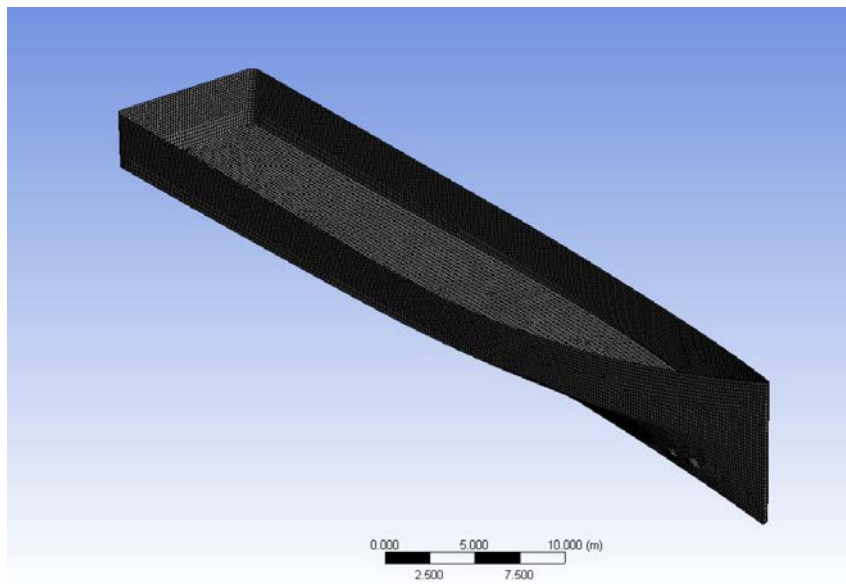
$$a_z = \omega^2 \zeta_a \frac{\sinh[k(z+h)]}{\sinh(kh)} \cos(kx - \omega t) \quad (22)$$

$$p_D = \rho g \zeta_a \frac{\cosh[k(z+h)]}{\cosh(kh)} \cos(kx - \omega t) \quad (23)$$

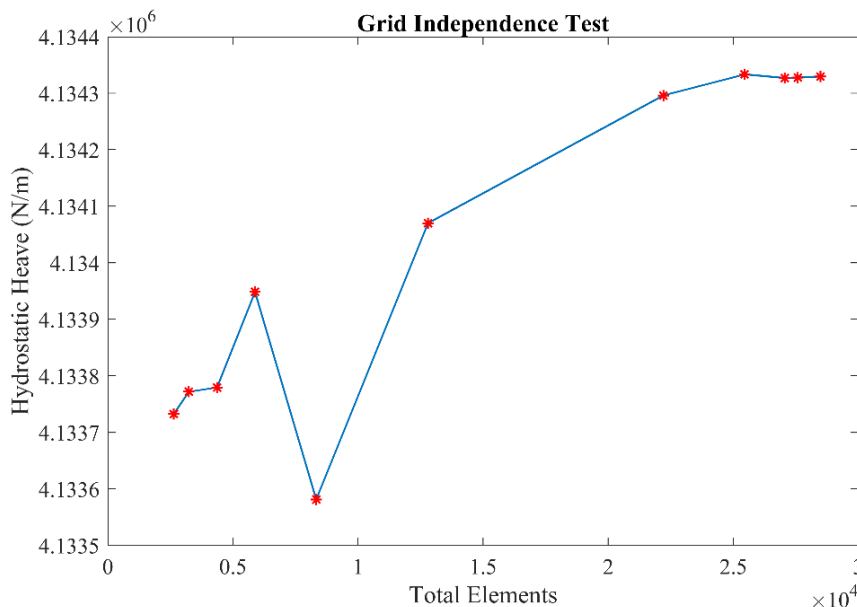
The term v_x and v_z are horizontal and vertical water particle velocity, a_x and a_z are horizontal and

Table 2.
Ship parameters in meshing process

Parameter	Value
Defeaturing tolerance (m)	0.15
Maximum element size (m)	0.35
Total nodes	22,484
Total elements	22,210
Density of water (kg/m ³)	1025
Water length and width (m)	[300; 200]
Gravitational acceleration (m/s ²)	9.81
Draught (m)	3.13
Breadth (m)	9.5
Length between perpendiculars (m)	53.25
Mass (kg)	600858
Radius of gyration (m)	[3.179; 13.313; 13.845]
Center of gravity (m)	[0; 0; 0]
Center of buoyancy (m)	[0; 0; 0.83]



(a)



(b)

Figure 5. Result of meshing process, (a) hull surface mesh; (b) grid independence test

vertical water particle acceleration, p_D is dynamic pressure, ρ is water density, ζ_a is wave height, t is time, and h is water depth. Impulse of the wave particles will cause motion of the ship hull. The equation of motion is expressed in a convolution integral form as equation (24),

$$(m + A_\infty)\ddot{X}(t) + c\dot{X}(t) + KX(t) + \int_0^t R(t - \tau)\dot{X}(\tau)d\tau = F(t) \quad (24)$$

The term m is structural mass matrix, A_∞ is fluid added mass matrix at infinite frequency, c is

damping matrix including the linear radiation damping effects, K is total stiffness matrix, R is velocity impulse function matrix, and X , \dot{X} , and \ddot{X} are respectively matrices of position, velocity, and acceleration of the ship. An integration of equation (24) is held numerically by Aqwa using parameters in Table 2.

Ship motion analysis is carried out in three classifications of ocean depth, such as shallow, intermediate, and deep waters, as shown in Table 3, which have an effect on the speed of ocean waves

Table 3. Random ocean waves parameters

Ocean classification	Depth (m)	Significant wave height (m)	Wave frequency (Hz)	Sea state
Shallow	50		0.50	
Intermediate	750	2	0.48	Moderate
Deep	3000		0.46	

Table 4.
Dynamic terms for azimuth angle

Term	Torque
Inertia	$\{I_{zz_1} + I_{xx_2} \sin^2 \theta_{l_2} + (I_{yy_2} + m_2 r_{x_2}^2) \cos^2 \theta_{l_2}\} \ddot{\theta}_{l_1}$ $+ \{-m_2 r_{x_2} \sin \theta_{l_1} \cos \theta_{l_2}\} \ddot{X}_S$ $+ \{m_2 r_{x_2} \cos \theta_{l_1} \cos \theta_{l_2}\} \ddot{Y}_S$ $+ \left\{ \frac{1}{2} (I_{xx_2} - I_{yy_2} - m_2 r_{x_2}^2) \cos \theta_{l_1} \sin 2 \theta_{l_2} \right\} \ddot{\phi}$ $+ \left\{ \frac{1}{2} (I_{xx_2} - I_{yy_2} - m_2 r_{x_2}^2) \sin \theta_{l_1} \sin 2 \theta_{l_2} \right\} \ddot{\psi}$ $+ \{I_{zz_1} + I_{xx_2} \sin^2 \theta_{l_2} + (I_{yy_2} + m_2 r_{x_2}^2) \cos^2 \theta_{l_2}\} \ddot{\psi}$
Coriolis	$\{(I_{xx_2} - I_{yy_2} - m_2 r_{x_2}^2) \sin 2 \theta_{l_2}\} \dot{\theta}_{l_1} \dot{\theta}_{l_2}$ $+ \{[(I_{xx_2} - I_{yy_2} - m_2 r_{x_2}^2) \cos 2 \theta_{l_2} - I_{zz_2} - m_2 r_{x_2}^2] \cos \theta_{l_1}\} \dot{\theta}_{l_2} \dot{\phi}$ $+ \{[(I_{xx_2} - I_{yy_2} - m_2 r_{x_2}^2) \cos 2 \theta_{l_2} - I_{zz_2} - m_2 r_{x_2}^2] \sin \theta_{l_1}\} \dot{\theta}_{l_2} \dot{\psi}$ $+ \{(I_{xx_2} - I_{yy_2} - m_2 r_{x_2}^2) \sin 2 \theta_{l_2}\} \dot{\theta}_{l_2} \dot{\psi}$ $+ \{m_2 r_{x_2} \cos \theta_{l_1} \cos \theta_{l_2}\} \dot{X}_S \dot{\psi}$ $+ \{m_2 r_{x_2} \sin \theta_{l_1} \cos \theta_{l_2}\} \dot{Y}_S \dot{\psi}$ $+ \{-m_2 r_{x_2} \cos \theta_{l_1} \cos \theta_{l_2}\} \dot{Z}_S \dot{\phi}$ $+ \{-m_2 r_{x_2} \sin \theta_{l_1} \cos \theta_{l_2}\} \dot{Z}_S \dot{\psi}$ $+ \{-[I_{xx_1} - I_{yy_1} - I_{zz_2} - m_2 r_{x_2}^2 + (I_{yy_2} + m_2 r^2) \sin^2 \theta_{l_2} + I_{xx_2} \cos^2 \theta_{l_2}] \cos 2 \theta_{l_1}\} \dot{\phi} \dot{\psi}$ $+ \left\{ \frac{1}{2} (I_{xx_2} - I_{yy_2} - m_2 r_{x_2}^2) \sin \theta_{l_1} \sin 2 \theta_{l_2} \right\} \dot{\phi} \dot{\psi}$ $+ \left\{ -\frac{1}{2} (I_{xx_2} - I_{yy_2} - m_2 r_{x_2}^2) \cos \theta_{l_1} \sin 2 \theta_{l_2} \right\} \dot{\phi} \dot{\psi}$
Centripetal	$\left\{ \frac{1}{2} [I_{xx_1} - I_{yy_1} - I_{zz_2} - m_2 r_{x_2}^2 + (I_{yy_2} + m_2 r_{x_2}^2) \sin^2 \theta_{l_2} + I_{xx_2} \cos^2 \theta_{l_2}] \sin 2 \theta_{l_1} \right\} \dot{\phi}^2$ $+ \left\{ -\frac{1}{2} [I_{xx_1} - I_{yy_1} - I_{zz_2} - m_2 r_{x_2}^2 + (I_{yy_2} + m_2 r_{x_2}^2) \sin^2 \theta_{l_2} + I_{xx_2} \cos^2 \theta_{l_2}] \sin 2 \theta_{l_1} \right\} \dot{\psi}^2$
Gravity	$m_2 g r_{x_2} \cos \theta_{l_2} (\sin \theta_{l_1} \sin \varphi + \cos \theta_{l_1} \sin \phi \cos \varphi)$

[30]. Equations (19)-(23) fortify that the kinematics of the wave particle is the function of ocean depth. Once the simulation is completed, six-DoF ship motion can be obtained and applied to the calculation in equation (11).

III. Results and Discussions

The results of the analytical derivation of manipulator joint torque using the Lagrange-Euler method are tabulated in Table 4 for the azimuth angle and Table 5 for the elevation angle. The equations are classified into dynamic terms for clarity. They have been validated by excluding the

terms of ship motions, and the results are similar to those without ship motions. Those terms are then utilized by substituting manipulator parameters in Table 6 and joint trajectories in Figure 6, which consist of both azimuth and elevation joints position, velocity, and acceleration over 30 s. The joint angles are obtained from the inverse kinematics process [31] and their trajectories are generated using the 5th-order spline function. As can be seen, smoothness of joint position, velocity, and acceleration can be obtained.

As mentioned in the previous section, ship motions are obtained using numerical simulation through hydrodynamic time response analysis in

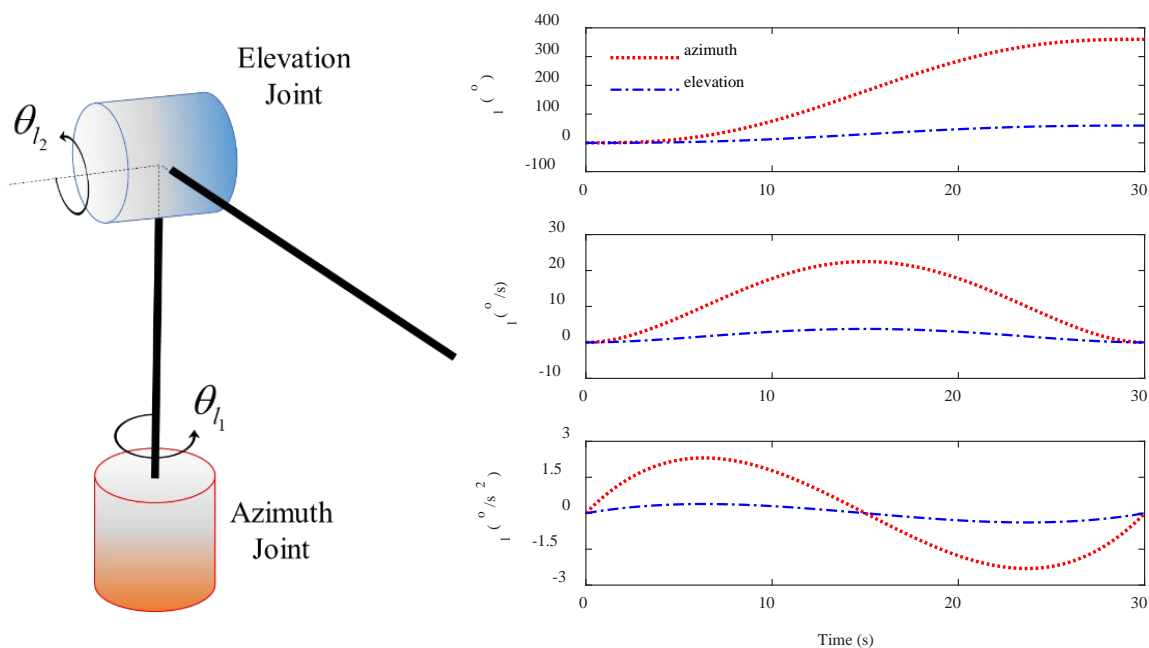


Figure 6. Manipulator joint trajectories

Table 5.
Dynamic terms for elevation angle

Term	Torque
Inertia	$\{I_{zz_2} + m_2 r_{x_2}^2\} \ddot{\theta}_{l_2}$ $+ \{-m_2 r_{x_2} \cos \theta_{l_1} \sin \theta_{l_2}\} \ddot{\chi}_S$ $+ \{-m_2 r_{x_2} \sin \theta_{l_1} \sin \theta_{l_2}\} \ddot{\psi}_S$ $+ \{m_2 r_{x_2} \cos \theta_{l_2}\} \ddot{Z}_S$ $+ \{(I_{zz_2} + m_2 r_{x_2}^2) \sin \theta_{l_1}\} \ddot{\phi}$ $+ \{-(I_{zz_2} + m_2 r_{x_2}^2) \cos \theta_{l_1}\} \ddot{\psi}$
Coriolis	$\{[-(I_{xx_2} - I_{yy_2} - m_2 r_{x_2}^2) \cos 2 \theta_{l_2} + I_{zz_2} + m_2 r_{x_2}^2] \cos \theta_{l_1}\} \dot{\theta}_{l_1} \dot{\phi}$ $+ \{[-(I_{xx_2} - I_{yy_2} - m_2 r_{x_2}^2) \cos 2 \theta_{l_2} + I_{zz_2} + m_2 r^2] \sin \theta_{l_1}\} \dot{\theta}_{l_1} \dot{\psi}$ $+ \{-(I_{xx_2} - I_{yy_2} - m_2 r_{x_2}^2) \sin 2 \theta_{l_2}\} \dot{\theta}_{l_1} \dot{\psi}$ $+ \{-m_2 r_{x_2} \cos \theta_{l_2}\} \dot{\chi}_S \dot{\phi}$ $+ \{-m_2 r_{x_2} \sin \theta_{l_1} \sin \theta_{l_2}\} \dot{\chi}_S \dot{\psi}$ $+ \{m_2 r_{x_2} \cos \theta_{l_2}\} \dot{\psi}_S \dot{\phi}$ $+ \{m_2 r_{x_2} \cos \theta_{l_1} \sin \theta_{l_2}\} \dot{\psi}_S \dot{\psi}$ $+ \{m_2 r_{x_2} \sin \theta_{l_1} \sin \theta_{l_2}\} \dot{Z}_S \dot{\phi}$ $+ \{-m_2 r_{x_2} \cos \theta_{l_1} \sin \theta_{l_2}\} \dot{Z}_S \dot{\psi}$ $+ \left\{ \frac{1}{2} (I_{xx_2} - I_{yy_2} - m_2 r_{x_2}^2) \sin 2 \theta_{l_1} \sin 2 \theta_{l_2} \right\} \dot{\phi} \dot{\psi}$ $+ \{-(I_{xx_2} - I_{yy_2} - m_2 r_{x_2}^2) \cos \theta_{l_1} \cos 2 \theta_{l_2}\} \dot{\phi} \dot{\psi}$ $+ \{-(I_{xx_2} - I_{yy_2} - m_2 r_{x_2}^2) \sin \theta_{l_1} \cos 2 \theta_{l_2}\} \dot{\psi} \dot{\psi}$
Centripetal	$\left\{ -\frac{1}{2} (I_{xx_2} - I_{yy_2} - m_2 r_{x_2}^2) \sin 2 \theta_{l_2} \right\} \theta_{l_1}^2$ $+ \left\{ \frac{1}{2} (I_{xx_2} - I_{yy_2} - m_2 r_{x_2}^2) \cos^2 \theta_{l_1} \sin 2 \theta_{l_2} \right\} \phi^2$ $+ \left\{ \frac{1}{2} (I_{xx_2} - I_{yy_2} - m_2 r_{x_2}^2) \sin^2 \theta_{l_1} \sin 2 \theta_{l_2} \right\} \psi^2$ $+ \left\{ -\frac{1}{2} (I_{xx_2} - I_{yy_2} - m_2 r_{x_2}^2) \sin 2 \theta_{l_2} \right\} \psi^2$
Gravity	$m_2 g r_{x_2} [\sin \theta_{l_2} (\cos \theta_{l_1} \sin \varphi - \sin \theta_{l_1} \sin \phi \cos \varphi) + \cos \theta_{l_2} \cos \phi \cos \varphi]$

Table 6.
Parameters of manipulator

Parameter	Value
Mass (kg)	$m_1 = 150; m_2 = 128$
Coordinates of CoG (m)	$r_{x1} = 0.00; r_{y1} = 0.19; r_{z1} = 0.00;$ $r_{x2} = 0.64; r_{y2} = 0.45; r_{z2} = 0.40$
Inertia moment at CoG (kg.m ²)	$I_{xx1} = 4.25; I_{yy1} = 5.45; I_{zz1} = 5.98;$ $I_{xy1} = 0.043; I_{yz1} = 0.553; I_{xz1} = 0.012;$ $I_{xx2} = 0.108; I_{yy2} = 14.745; I_{zz2} = 14.74;$ $I_{xy2} = 0.083; I_{yz2} = 0.002; I_{xz2} = 0.019$
Gravity (m/s ²)	$g_x = 0; g_y = 0; g_z = 9.81$

ANSYS Aqwa subject to the three ocean depths. As part of the hydrodynamic response study, an exhaustive time domain response analysis examines the various effects of irregular wave loads on the dynamic responses of the ship [32]. Figure 7 shows three time series of ocean wave height and its corresponding six-DoF ship motion. It is clearly seen that the wave height is inversely proportional to the ocean depth following equation (20) and equation (22). Shallow water produces higher ocean wave height so that the amplitudes of the surge, sway, and yaw motions become higher than the other motions. On the contrary, the dynamic pressure of the ocean wave is directly proportional to the ocean depth following equation (23), implying that lifting motions such as heave, roll, and pitch have higher amplitudes in deep water. Those results are then fed into dynamic terms in Table 4 and Table 5, along with predefined joint trajectories.

Torque comparisons between an undisturbed manipulator (without ship motions) and a disturbed manipulator (with ship motions) in shallow water are then investigated and displayed in Figure 8 and Figure 9, respectively. Those figures present the distributions of joint torque for each dynamic term

of azimuth and elevation links. As can be observed, the inertia term is the most dominant torque to the manipulator for the azimuth link, while the gravity term is found to be dominant in the elevation link. This is to be expected since gravity works on the axis of rotation of the elevation link. Further, a comparison between undisturbed and disturbed manipulators under variations of ocean depth is revealed in Figure 10. It is apparent that the ship motions greatly affect the values of manipulator joint torque.

The values fluctuate around the value of the undisturbed manipulator for all ocean depths, become unstable and increase to certain maximum values in order to maintain the position of the end-effector. It is found that shallow water produces the highest torque value in azimuth angle, where the increment is around 8.271 N.m or 285.69 % from the undisturbed manipulator. Intermediate water produces the highest torque in elevation angle, where the increment is around 53.321 N.m or 6.63 %. The performance of manipulator joints in terms of angular speed and torque is then compiled in Table 7 to support the results in Figure 10.

This is to be expected since shallow water produces the highest amplitude in yaw motion, which is the variable of the inertia term in azimuth

angle. The maximum torque of elevation angle is produced in intermediate water depth because the highest amplitude in roll motion is achieved in

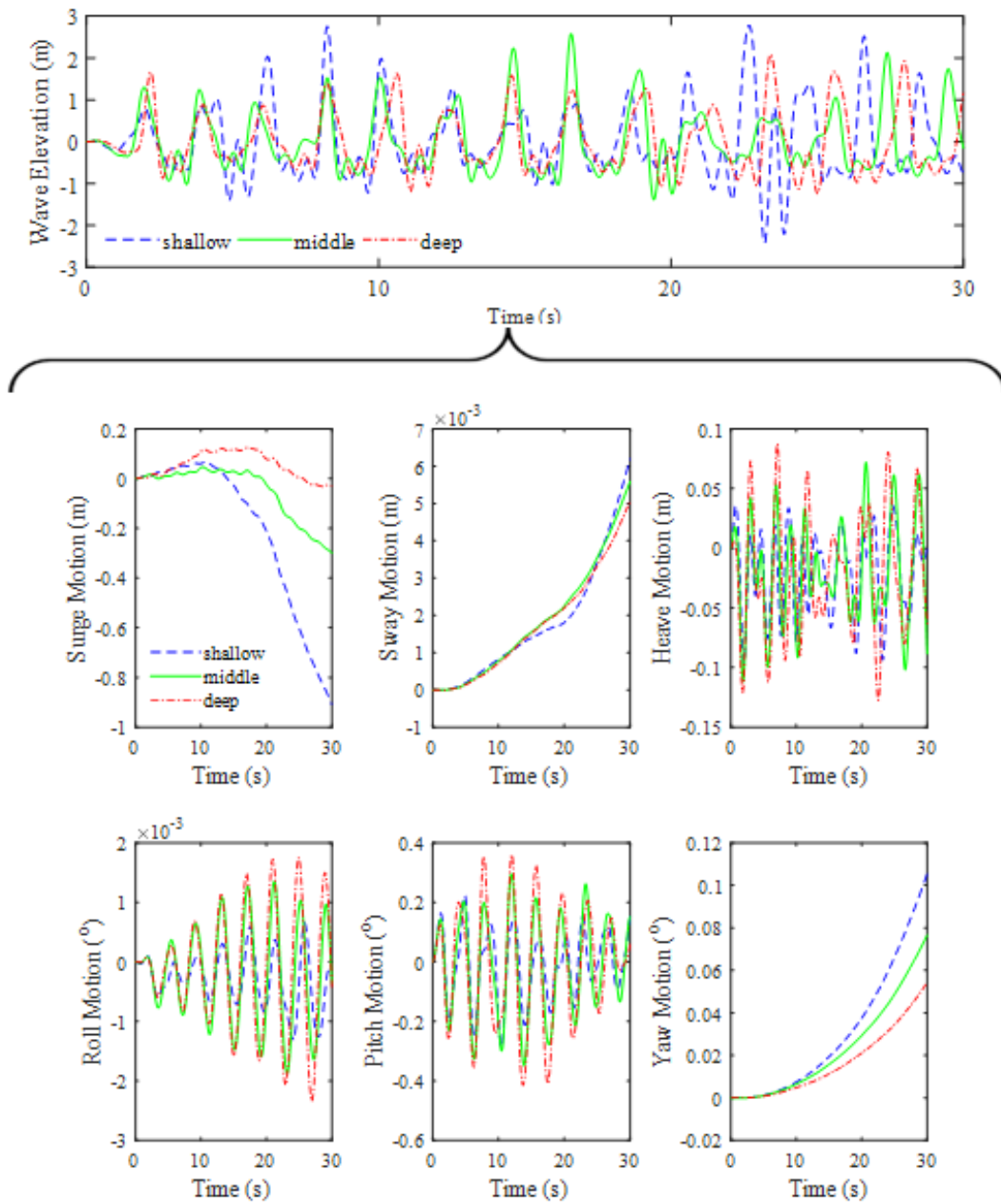


Figure 7. Ship motions subject to ocean depth variation

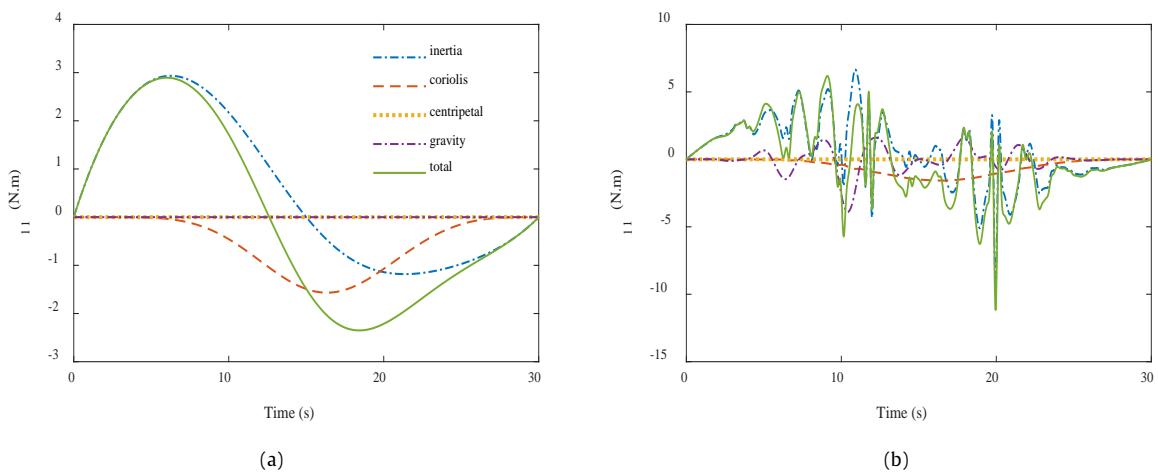


Figure 8. Azimuth torque distribution: (a) undisturbed; (b) in shallow water

intermediate water depth in the first 7 s of response since gravity term, as the main contributor of the elevation angle, contains roll motion. The results

show that maximum torque between applied ocean depth variations has small differences.

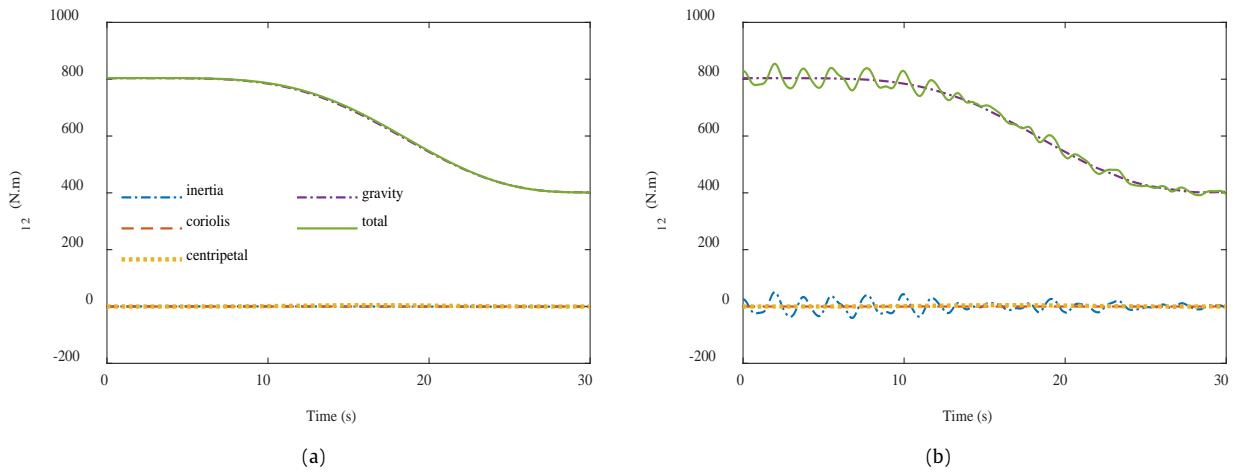


Figure 9. Elevation torque distribution: (a) undisturbed; (b) in shallow water

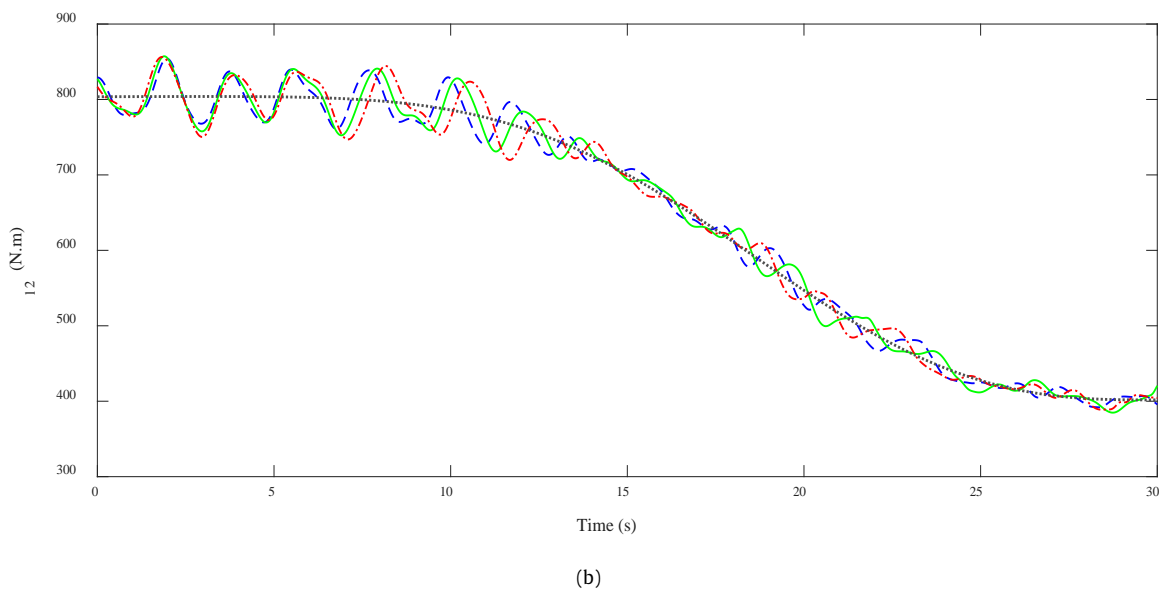
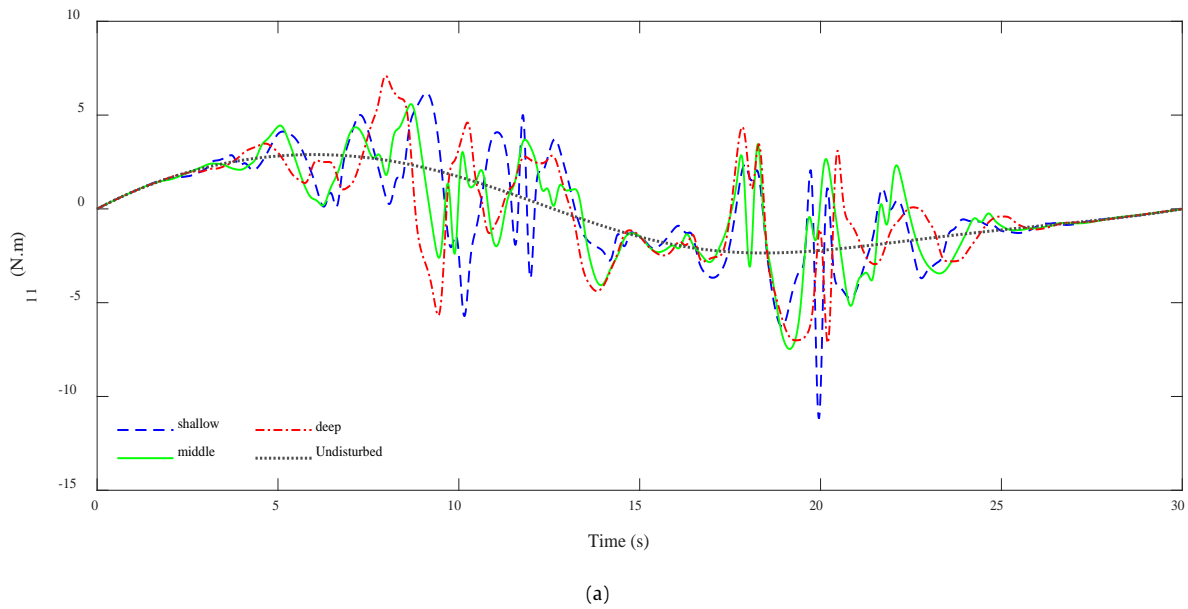


Figure 10. Dynamic joint torques: (a) azimuth; (b) elevation

Table 7.
Manipulator Torque Performance

Manipulator joint	Performance			
	Undisturbed	Ocean depth		
		Shallow	Intermediate	Deep
Azimuth	$\omega_{l_1} = 22.492 \text{ }^\circ/\text{s}$			
	$\tau_{l_1} = 2.895 \text{ N.m}$	$\tau_{l_1} = 11.166 \text{ N.m}$	$\tau_{l_1} = 7.468 \text{ N.m}$	$\tau_{l_1} = 7.147 \text{ N.m}$
Elevation	$\omega_{l_2} = 3.749 \text{ }^\circ/\text{s}$			
	$\tau_{l_2} = 803.943 \text{ N.m}$	$\tau_{l_2} = 854.261 \text{ N.m}$	$\tau_{l_2} = 857.264 \text{ N.m}$	$\tau_{l_2} = 856.325 \text{ N.m}$

IV. Conclusion

A ship-mounted two-DoF manipulator dynamics under the variations of ocean depth have been investigated in this paper. The results are obtained by combining the mathematical model of the manipulator system with the numerical simulation of ship motions. Finding results show that randomness of ship motions appears in joint torque in terms of oscillations, resulting in higher maximum torque values than the manipulator without ship motions. Shallow water produces maximum joint torque to the azimuth angle with an increment of 8.271 N.m (285.69 %) from the undisturbed manipulator. Meanwhile, intermediate water produces a maximum joint torque value to the elevation angle with an increment of 53.321 N.m (6.63 %). However, the difference between water depth variations is relatively small. Current results can be taken as a baseline for sizing the electrical motor of the manipulator system and the development of a robust control system. Experimental work is recommended as future work to validate simulation results.

Acknowledgements

The authors are grateful to the National Research and Innovation Agency (BRIN), especially Research Center for Smart Mechatronics for providing the research facility and also to the Ministry of Finance of the Republic of Indonesia for financial support through the LPDP scheme with the project no. PRJ-92/LPDP/2020.

Declarations

Author contribution

M.L. Ramadiansyah: Writing - Original Draft, Writing - Review & Editing, Conceptualization, Investigation, Visualization, Data Curation. E. Yazid: Writing - Review & Editing, Conceptualization, Supervision, Validation, Funding acquisition. C.Y. Ng: Formal analysis, Resources, Software, Validation, Visualization.

Funding statement

This research did not receive any specific grant from funding agencies in the public, commercial, or not-for-profit sectors.

Competing interest

The authors declare that they have no known competing financial interests or personal relationships that could have appeared to influence the work reported in this paper.

Additional information

Reprints and permission: information is available at <https://mev.lipi.go.id/>.

Publisher's Note: National Research and Innovation Agency (BRIN) remains neutral with regard to jurisdictional claims in published maps and institutional affiliations.

References

- [1] T. Lauß, S. Oberpeilsteiner, K. Sherif, and W. Steiner, "Inverse dynamics of an industrial robot using motion constraints," in *2019 20th International Conference on Research and Education in Mechatronics (REM)*, pp. 1-7, 2019.
- [2] N. Ramadhan, N. Lilansa, A. Rifa'i, and H. Nguyen, "Pattern recognition based movement control and gripping forces control system on arm robot model using LabVIEW," *Journal of Mechatronics, Electrical Power, and Vehicular Technology*, vol. 13, no. 1, pp. 1-14, 2022.
- [3] S. K. Deb, J. H. Rokky, T. C. Mallick, and J. Shetara, "Design and construction of an underwater robot," in *2017 4th International Conference on Advances in Electrical Engineering (ICAEE)*, pp. 281-284, 2017.
- [4] Y. Zhao et al., "A vehicle handling inverse dynamics method for emergency avoidance path tracking based on adaptive inverse control," *IEEE Trans Veh Technol*, vol. 70, no. 6, pp. 5470-5482, 2021.
- [5] M. Reza Chalak Qazani, H. Asadi, S. Mohamed, S. Nahavandi, J. Winter, and K. Rosario, "A Real-Time Motion Control Tracking Mechanism for Satellite Tracking Antenna Using Serial Robot," in *2021 IEEE International Conference on Systems, Man, and Cybernetics (SMC)*, pp. 1049-1055, 2021.
- [6] K. Kaneko et al., "Humanoid Robot HRP-5P: An electrically actuated humanoid robot with high-power and wide-range joints," *IEEE Robot Autom Lett*, vol. 4, no. 2, pp. 1431-1438, 2019.
- [7] Z. Huang, X. Jiang, H. Liu, X. Chen, T. Fukuda, and Q. Huang, "Design of crawling motion for a biped walking humanoid with 3-DoF rigid-flexible waist," in *2018 IEEE-RAS 18th International Conference on Humanoid Robots (Humanoids)*, pp. 974-979, 2018.
- [8] F. Tavassolian, H. Khotanlou, and P. Varshovi-Jaghargh, "Forward kinematics analysis of a 3-PRR planar parallel robot using a combined method based on the neural network," in *2018 8th International Conference on Computer and Knowledge Engineering (ICCKE)*, pp. 320-325, 2018.
- [9] W. Dewandhana, K. I. Apriandy, B. S. B. Dewantara, and D. Pramadihanto, "Forward kinematics with full-arm analysis on 'T-Flow' 3.0 Humanoid Robot," in *2021 International Electronics Symposium (IES)*, pp. 356-361, 2021.
- [10] D. Kusmenko and K. Schmidt, "Development of an analytical inverse kinematics for a 5 DOF manipulator," in *2020 21st International Conference on Research and Education in Mechatronics (REM)*, pp. 1-5, 2020.

- [11] P. Chen, J. Long, W. Yang, and J. Leng, "Inverse kinematics solution of underwater manipulator based on Jacobi matrix," in *OCEANS 2021: San Diego - Porto*, pp. 1-4, 2021.
- [12] M. F. Amundsen, J. Sverdrup-Thygeson, E. Kelasidi, and K. Y. Pettersen, "Inverse kinematic control of a free-floating underwater manipulator using the generalized Jacobian matrix," in *2018 European Control Conference (ECC)*, pp. 276-281, 2018.
- [13] A. S. Polydoros, E. Boukas, and L. Nalpantidis, "Online multi-target learning of inverse dynamics models for computed-torque control of compliant manipulators," in *2017 IEEE/RSJ International Conference on Intelligent Robots and Systems (IROS)*, pp. 4716-4722, 2017.
- [14] A. Awatef and B. H. Mouna, "Dynamic modeling and inverse dynamic control of mobile robot," in *2017 International Conference on Green Energy Conversion Systems (GECS)*, pp. 1-5, 2017.
- [15] F. Crenna and G. B. Rossi, "Measurement uncertainty evaluation in biomechanical inverse dynamics analysis," in *2020 IEEE International Instrumentation and Measurement Technology Conference (I2MTC)*, pp. 1-5, 2020.
- [16] E. Farah and L. Shaogang, "An efficient approach for manipulator robot dynamics modeling," in *2018 International Conference on Computer, Control, Electrical, and Electronics Engineering (ICCCEEE)*, pp. 1-5, 2018.
- [17] A. Müller, "Recursive second-order inverse dynamics for serial manipulators," in *2017 IEEE International Conference on Robotics and Automation (ICRA)*, pp. 2483-2489, 2017.
- [18] B. Wei, Y. Li, Y. Zhang, Y. Li, and S. Shu, "Dynamic modeling of mobile manipulator based on floating-like base," in *2022 IEEE 6th Information Technology and Mechatronics Engineering Conference (ITOEC)*, vol. 6, pp. 993-998, 2022.
- [19] R. Szász, M. Allenspach, M. Han, M. Tognon, and R. K. Katschmann, "Modeling and control of an omnidirectional micro aerial vehicle equipped with a soft robotic arm," in *2022 IEEE 5th International Conference on Soft Robotics (RoboSoft)*, pp. 1-8, 2022.
- [20] Y. Cai, S. Zheng, W. Liu, Z. Qu, and J. Han, "Model analysis and modified control method of ship-mounted stewart platforms for wave compensation," *IEEE Access*, vol. 9, pp. 4505-4517, 2021.
- [21] W. Lv, L. Tao, and Z. Ji, "Design and control of cable-drive parallel robot with 6-dof active wave compensation," in *2017 3rd International Conference on Control, Automation and Robotics (ICCAR)*, pp. 129-133, 2017.
- [22] X. Huang, J. Wang, Y. Xu, Y. Zhu, T. Tang, and F. Xu, "Dynamic modeling and analysis of wave compensation system based on floating crane in smart port," in *2018 International Symposium in Sensing and Instrumentation in IoT Era (ISSI)*, pp. 1-5, 2018.
- [23] Y. Qian and Y. Fang, "Dynamics analysis of an offshore ship-mounted crane subject to sea wave disturbances," in *2016 12th World Congress on Intelligent Control and Automation (WCICA)*, pp. 1251-1256, 2016.
- [24] E. Yazid, A. S. Nugraha, H. M. Saputra, and Rahmat, "Dynamics of a ship-mounted two-DoF manipulator case: effect of sea state to the manipulator joint torque," in *2019 IEEE International Conference on Industry 4.0, Artificial Intelligence, and Communications Technology (IAICT)*, pp. 1-6, 2019.
- [25] M. O. Ahmed, A. Yenduri, and V. J. Kurian, "Evaluation of the dynamic responses of truss spar platforms for various mooring configurations with damaged lines," *Ocean Engineering*, vol. 123, pp. 411-421, 2016.
- [26] Y. Cai, S. Zheng, W. Liu, Z. Qu, and J. Han, "Model analysis and modified control method of ship-mounted stewart platforms for wave compensation," *IEEE Access*, vol. 9, pp. 4505-4517, 2021.
- [27] J. Yue, "Kinematic modelling and simulation of LeArm robot," in *2022 6th International Conference on Robotics, Control and Automation (ICRCA)*, pp. 1-6, 2022.
- [28] E. Yazid, R. Ristiana, M. Mirdanies, R. A. Ardiansyah, R. Rahmat, and Y. Sulaeman, "Sizing the mechanical and electrical performances of a two-DoF manipulator design taking into account PMSM type three-phase AC servo motor," in *2021 International Conference on Computer Science and Engineering (IC2SE)*, vol. 1, pp. 1-9, 2021.
- [29] S. Son, "Design of ocean platforms against ringing response," Master of Science Thesis in Mechanical Engineering, Texas Tech University, 2006.
- [30] P. Webb, "Introduction to oceanography," *Roger Williams University*, Aug. 2021. [accessed: Aug. 20, 2022].
- [31] E. Yazid, M. Mirdanie, R. A. Ardiansyah, Rahmat, R. Ristiana, and Y. Sulaeman, "Inverse kinematics model for a ship mounted two-DoF manipulator system," in *2021 IEEE Ocean Engineering Technology and Innovation Conference: Ocean Observation, Technology and Innovation in Support of Ocean Decade of Science (OETIC)*, pp. 50-56, 2021.
- [32] R. D. Fernandes and R. Sundaravavelu, "Hydrodynamic response of floating pontoon for seaplane operation," in *OCEANS 2022 - Chennai*, pp. 1-10, 2022.